DETC2002/MECH-34245

MODIFIED 6-PSU PLATFORM

Brian R. Hopkins and **Robert L. Williams II**
Ohio University
Athens, OH 45701

ABSTRACT

The Department of Mechanical Engineering at Ohio University has designed, constructed, and controlled a new 6-dof in-parallel-actuated platform, a combination and modification of existing designs. The 6-PSU platform consists of 6 legs with a prismatic joint, spherical joint, and universal joint connecting links in each leg which move the platform in the six Cartesian freedoms with respect to the base. The prismatic joint is actuated while the other two joints in each leg are passive. The six prismatic joints move vertically with respect to the base, which appears to be a big improvement over the standard Gough/Stewart platform. Experimental results from the Ohio University manipulator are presented.

1. INTRODUCTION

The Stewart/Gough platform (Stewart, 1966), arguably the most popular platform manipulator, is a 6-dof platform controlled by six active prismatic joints. Six UPS legs connect the fixed base to the moving platform (universal U, prismatic P, spherical S joints; underlining indicates that joint is active, while the others are passive).

Merlet and Gosselin (1991) first proposed a 6-PUS platform manipulator, with a major advantage over the Stewart/Gough platform: all active prismatic joints move with respect to the base and hence are not articulating; there are articulating links, but these are of fixed length. Stoughton and a team from Sandia, NIST, and Case Western have recently built a 6-PUS platform named the *ParaDex* (Kozlowski and Stoughton website, 2001); this was proposed for surgery, and then implemented for fixturing at Ford. Wang et al. (2000) presented *ParaDex* Workspace analysis. Bonev and Ryu (1999) also present workspace analysis and an extensive literature review for general 6-dof PUS parallel manipulators (called *HexaSlide* by these authors), of which the *ParaDex* is a

member. Kim and Ryu (2000) derived closed-form dynamics equations for general 6-dof PUS parallel manipulators.

Our 6-PSU design (kinematically equivalent to the 6-PUS by Merlet and Gosselin, 1991) is a modification of the *ParaDex*, wherein the moving and fixed platforms have their U and P joints, respectively, mounted in two concentric circles, rather than one circle as in the *ParaDex*, to improve dexterity. This idea came from Stoughton (Stoughton et al., 1993), originally for the Gough/Stewart platform. So, we have combined many good ideas into a new type of parallel platform manipulator. Applications include robotic surgery, haptic interface, flight simulator, motion platform, vibration isolation, and industrial robotics. Fig. 1 shows our CAD model and Fig. 2 shows the Ohio University hardware.
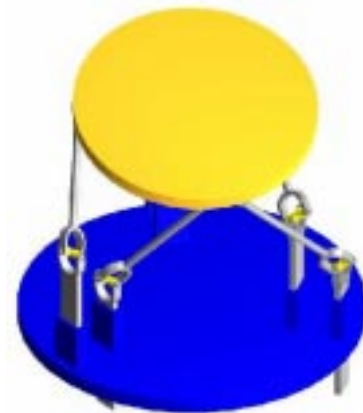

Figure 1. Modified 6-PSU CAD Model

This paper first presents our 6-PSU model, followed by kinematic equations and workspace determination, manipulator design and construction, control, and then experimental results.

Figure 2. Modified 6-PSU Prototype

2. 6-PSU MODEL

The 6-PSU manipulator kinematic diagram is shown below in Figs. 3 and 4. Six PSU legs connect the base and moving platform. Each leg consists of a linear actuator (prismatic joint P), a spherical joint S, a rigid link, and a universal joint U. The linear actuators are attached to the base, and the universal joints are attached to the moving platform. The base coordinate frame $\{B\}$, the moving platform coordinate frame $\{P\}$, and the joint locations on these platforms are shown in Fig. 4.
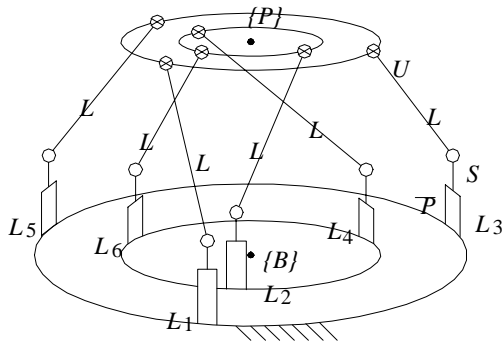

Figure 3. 6-PSU Kinematic Diagram

3. KINEMATICS

Inverse pose kinematics (given the Cartesian values, $X=\{x,y,z,\theta_z,\theta_y,\theta_x\}^T$, calculate the leg lengths L_1, L_2, L_3, L_4, L_5, and L_6) is required for control of the platform, and forward pose kinematics (given the leg lengths, calculate the Cartesian values) is useful for motion simulation. The vector-loop-closure diagram for both types of pose kinematics problems is given in Fig. 5. For clarity, Fig. 5 does not show the concentric joint locations of Figs. 3 and 4.

3.1 6-PSU Inverse Pose Kinematics

The 6-PSU inverse pose kinematics problem is stated: Given X, find L_i. The following vector loop-closure equation for each leg is written from Fig. 5.

$$^B B_i + {}^B L_i + {}^B A_i = \begin{Bmatrix} x \\ y \\ z \end{Bmatrix} + {}^B_P R\, {}^P P_i \quad i = 1, 2 \ldots 6 \quad (1)$$
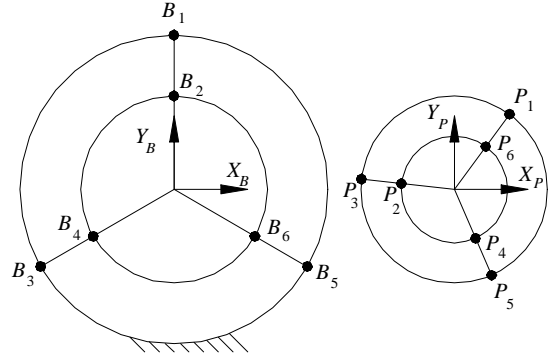

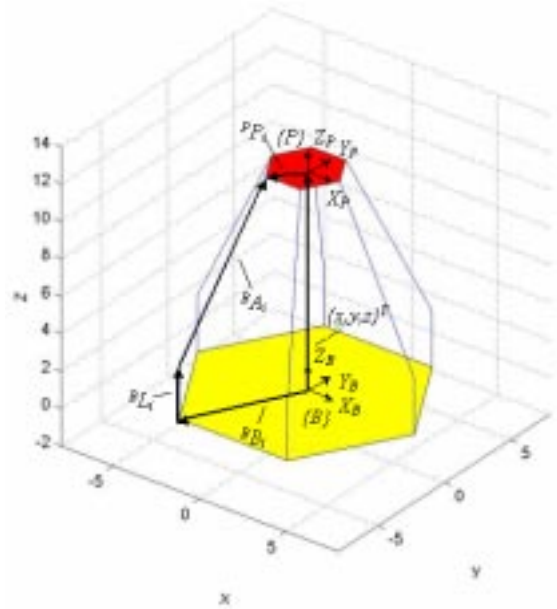*Figure 4. 6-PSU Base and Moving Platform Details*

Figure 5. Vector-Loop-Closure Diagram

Equation (1) is then expanded and simplified.

$$\begin{Bmatrix} B_{ix} \\ B_{iy} \\ 0 \end{Bmatrix} + \begin{Bmatrix} 0 \\ 0 \\ L_i \end{Bmatrix} + \begin{Bmatrix} A_{ix} \\ A_{iy} \\ A_{iz} \end{Bmatrix} = \begin{Bmatrix} x \\ y \\ z \end{Bmatrix} + \begin{bmatrix} r_{11} & r_{12} & r_{13} \\ r_{21} & r_{22} & r_{23} \\ r_{31} & r_{32} & r_{33} \end{bmatrix} \begin{Bmatrix} P_{ix} \\ P_{iy} \\ 0 \end{Bmatrix} \quad (2)$$

Given X, the spatial pose of the moving platform is completely determined. Rows 1 and 2 of equation (2) are solved algebraically for A_{ix} and A_{iy}.

$$A_{ix} = x + r_{11}P_{ix} + r_{12}P_{iy} - B_{ix} \tag{3}$$

$$A_{iy} = y + r_{21}P_{ix} + r_{22}P_{iy} - B_{iy} \tag{4}$$

Row 3 of Equation 2 contains two unknowns, however. Since the magnitude of ${}^{B}A_i$ is constant, the Euclidean Norm is used to solve for A_{iz}.

$$A_{iz} = \pm\sqrt{\left|{}^{B}A_i\right|^2 - A_{ix}^2 - A_{iy}^2} \tag{5}$$

L_i is now solved using row 3 of Equation 2.

$$L_i = z + r_{31}P_{ix} + r_{32}P_{iy} - A_{iz} \tag{6}$$

Since two solutions exist for A_{iz}, two corresponding solutions exist for L_i. The six legs, with two solutions each, results in 64 inverse kinematic solutions. In practical application, interference between the legs and the moving platform make the second solution for each leg unreachable; therefore only one of these 64 solutions is useful for a given manipulator. Therefore, L_i corresponding to the positive A_{iz} in Equation 5 are used for all legs.

3.2 6-PSU Forward Pose Kinematics

The 6-PSU forward pose kinematics problem is stated: Given L_i, find X. Vector loop-closure equation (1) again applies. The Newton-Raphson numerical method is used to find the solution. Equation (2) is rewritten and expanded.

$$\begin{bmatrix} A_{ix} \\ A_{iy} \\ A_{iz} \end{bmatrix} = \begin{Bmatrix} x + r_{11}P_{ix} + r_{12}P_{iy} - B_{ix} \\ y + r_{21}P_{ix} + r_{22}P_{iy} - B_{iy} \\ z + r_{31}P_{ix} + r_{32}P_{iy} - L_i \end{Bmatrix} \quad i = 1,2...6 \tag{7}$$

The constant length A_i of the passive leg is the Euclidean Norm of the vector in equation (7).

$$A_i^2 = A_{ix}^2 + A_{iy}^2 + A_{iz}^2 \tag{8}$$

Rows 1, 2, and 3 of equation (7) are then substituted into equation (8), which is expanded, simplified, and rearranged into the following form.

$$\begin{aligned} f_i(X) &= x^2 + y^2 + z^2 + r_{Pi}^2 + r_{Bi}^2 + L_i^2 \\ &+ 2(P_{ix}r_{11} + P_{iy}r_{12})(x - B_{ix}) + 2(P_{ix}r_{21} + P_{iy}r_{22})(x - B_{iy}) \\ &+ 2(P_{ix}r_{31} + P_{iy}r_{32})(z - L_i) - 2(xB_{ix} + yB_{iy} + zL_i) - A_i^2 = 0 \end{aligned} \tag{9}$$

Next, the Newton-Raphson Jacobian matrix is found by taking the partial derivatives of $f_i(X)$ with respect to each unknown in the function, X_j.

$$J_{NR}(i, j) = \frac{\partial f_i}{\partial X_j} \tag{10}$$

This results in the 6x6 Newton-Raphson Jacobian matrix (11).

An initial guess is made and equation (12) is used to update the solution. This initial guess must be close to the actual solution for the Newton-Raphson method to converge, but convergence is not guaranteed. Also, only one of the multiple solutions will be found, generally closest to the initial guess.

$$\begin{aligned} J_{NR}(i,1) &= 2[x + P_{ix}r_{11} + P_{iy}r_{12} - B_{ix}] \\ J_{NR}(i,2) &= 2[y + P_{ix}r_{21} + P_{iy}r_{22} - B_{iy}] \\ J_{NR}(i,3) &= 2[z + P_{ix}r_{31} + P_{iy}r_{32} - L_i] \\ J_{NR}(i,4) &= 2[-(P_{ix}r_{21} + P_{iy}r_{22})(x - B_{ix}) + (P_{ix}r_{11} + P_{iy}r_{12})(y - B_{iy})] \\ J_{NR}(i,5) &= 2\begin{bmatrix} (-P_{ix}c_z s_y + P_{iy}c_z r_{32})(x - B_{ix}) \\ +(-P_{ix}s_z s_y + P_{iy}s_z r_{32})(y - B_{iy}) - (P_{ix}c_y + P_{iy}s_z s_x)(z - L_{ix}) \end{bmatrix} \\ J_{NR}(i,6) &= 2[P_{iy}r_{13}(x - B_{ix}) + P_{iy}r_{23}(y - B_{iy}) + P_{iy}r_{33}(z - L_i)] \end{aligned} \tag{11}$$

$$\{X_{k+1}\} = \{X_k\} - [J_{NR}(X_k)]^{-1}\{f_i(X_k)\} \tag{12}$$

3.3 6-PSU Coordinate Frame Offset

The model in Figs. 3 and 4 does not completely describe the actual hardware manipulator shown in Fig. 2. An offset exists between the moving platform coordinate frame $\{P\}$ (on the plane of the six U-joints) and the coordinate frame placed at the top center of the actual moving platform $\{H\}$. This offset is described in Fig. 6. The orientation of $\{P\}$ and $\{H\}$ always match.
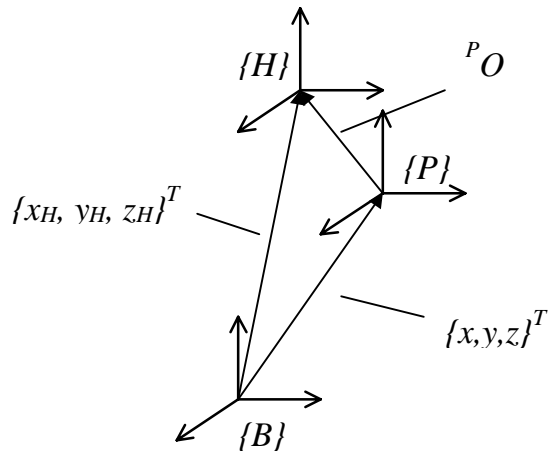

Figure 6. Offset Vector-Loop-Closure Diagram

The vector-loop-closure equation for the coordinate frame offset is written in equation (13); this must be used at the end of forward pose kinematics and at the beginning of inverse pose kinematics.

$$\begin{Bmatrix} x_H \\ y_H \\ z_H \end{Bmatrix} = \begin{Bmatrix} x \\ y \\ z \end{Bmatrix} + {}^{B}_{P}R\,{}^{P}O \tag{13}$$

3.4 6-PSU Workspace Determination

The workspace of a manipulator can be defined in two ways: reachable workspace and dexterous workspace. The reachable workspace is the collection of all points $\{x,y,z\}^T$ that can be reached by the manipulator in any orientation. The dexterous workspace is the collection of all points that can be reached by a manipulator in all orientations. Consequently, the dexterous workspace is always a subset of the reachable workspace. It is well known for most parallel manipulators that the dexterous workspace is null, since these manipulators cannot reach all orientations at any position in the reachable workspace. Therefore, dexterous workspace is defined in this paper to be the collection of all points that can be reached by a manipulator over a given set of desired orientations.

Factors that limit the workspace of a given parallel manipulator include actuator limits, leg interference, and singularities. In determining the workspace of the 6-PSU manipulator in this paper, only actuator limits are considered.

To determine the workspace of the 6-PSU manipulator, the inverse pose kinematic solution is calculated over a range of desired poses. All real solutions within the actuator limits are collected to form the dexterous workspace.

The reachable and dexterous workspaces for our final 6-PSU design are shown in Figs. 7 and 8. The dexterous workspace for this simulation requires that the manipulator be able to reach ±30° in all three Euler angles simultaneously; we use *Z-Y-X* Euler angle convention (Craig, 1989). An improved angular convention is proposed by Bonev and Ryu (1999); we have not used this yet, but will investigate it in the future. Each sub-picture is a top view of a horizontal 152.4 by 152.4 *mm* (6 by 6 *in*) slice of the workspace. The top left corner is the lowermost portion of the workspace. Advancing from left-to-right and top-to-bottom moves up in the workspace; each slice is 12.7 *mm* (½ *in*) above the previous slice.
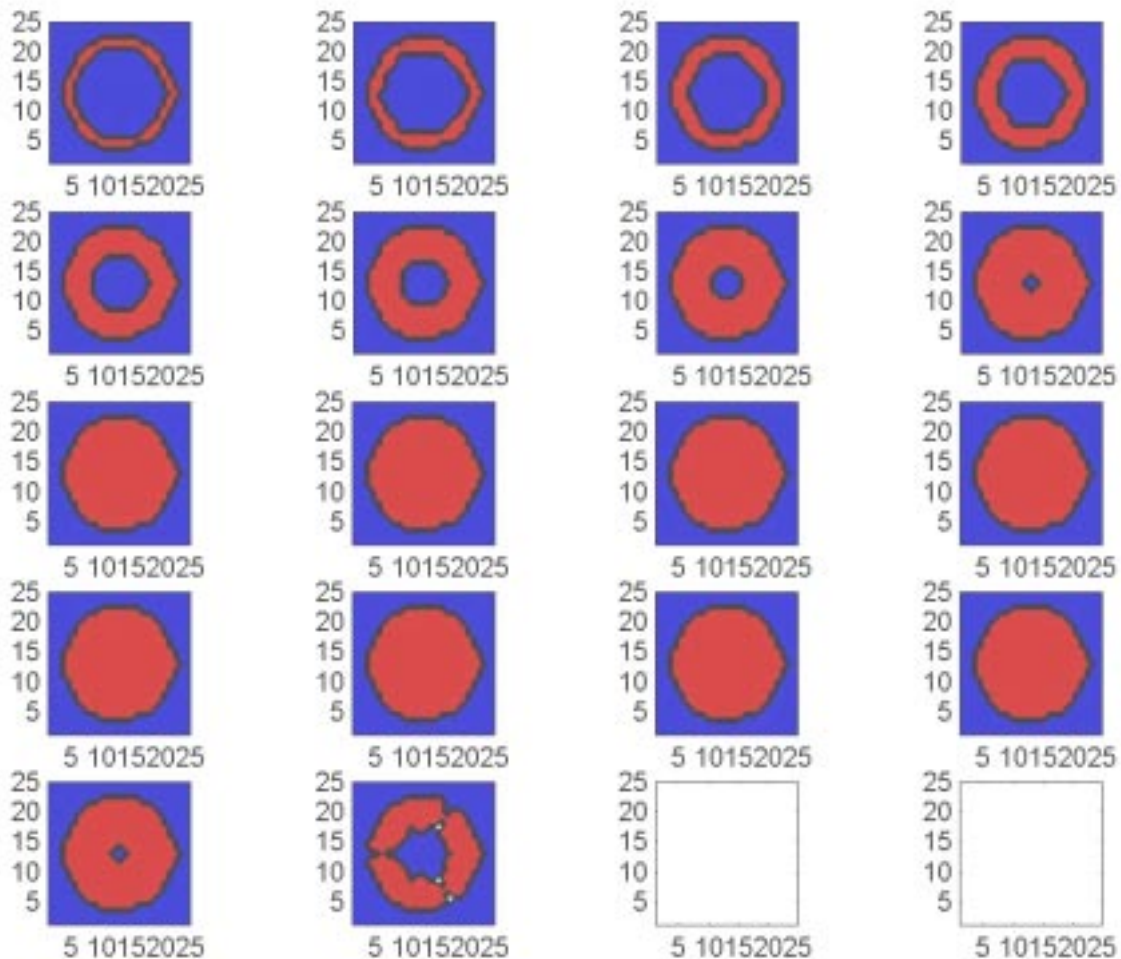

Figure 7. 6-PSU Reachable Workspace

4

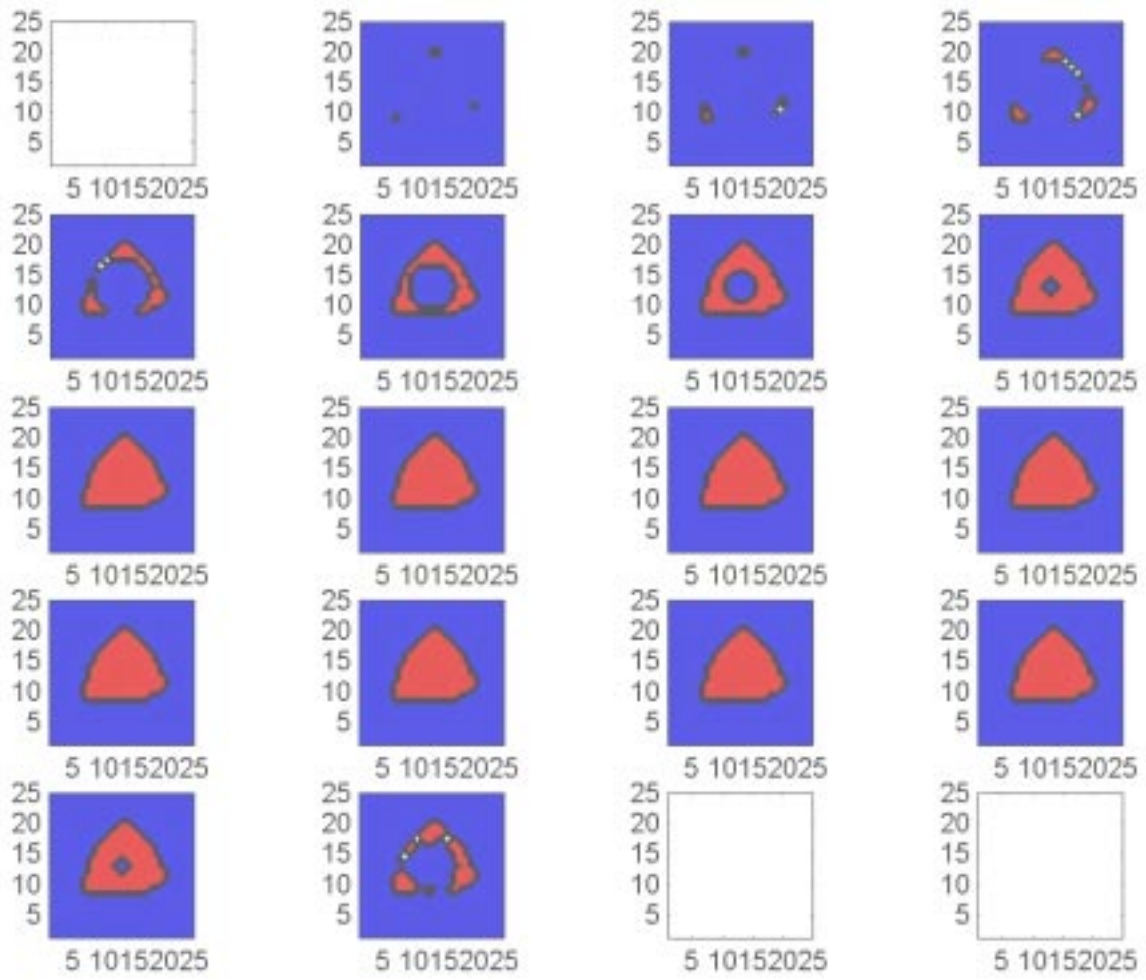*Figure 8. 6-PSU ±30° Dexterous Workspace*

4. 6-PSU DESIGN AND CONSTRUCTION

The prototype 6-PSU manipulator in Fig. 9 was intended to be a general-purpose manipulator; therefore, dexterous workspace was the most important factor in the selection of manipulator geometry. An acceptable workspace was to be large enough to visually demonstrate Cartesian motion in all six degrees-of-freedom, and be regular in shape. Workspace analysis was employed to help determine the manipulator geometry. The base platform joint locations, passive legs' length $\left| {}^{B}A_i \right|$, and moving platform joint locations were the design variables. Many different platform designs were considered, and symmetry was maintained in every case. Workspace analysis was performed for each design, and trends were noted. The geometry was finalized when an acceptable workspace was produced.

In the final hardware design, the moving platform universal joint locations are aligned on concentric circles as shown in Fig. 4 (right) of radii 50 *mm* and 80 *mm*. The base prismatic joints are also aligned on concentric circles as shown in Fig. 4 (left) of radii 100 *mm* and 165 *mm*. All pairs of base and platform joints in Fig. 4 are placed symmetrically and aligned radially, spaced by 120°. The six passive links each connect points B_i and P_i. The configuration of Fig. 4 shows the nominal configurations where all active leg lengths are equal; $\{B\}$ and $\{P\}$ have the same orientation in these cases, but the platform joints' alignment is as shown in Fig. 4 (the P_1P_6 radius is aligned 33.7° CW from the Y_P axis). The passive leg lengths are all $\left| {}^{B}A_i \right| = 225$ *mm*, and the offset between $\{H\}$ and $\{P\}$ is ${}^{P}O = 47$ *mm*.
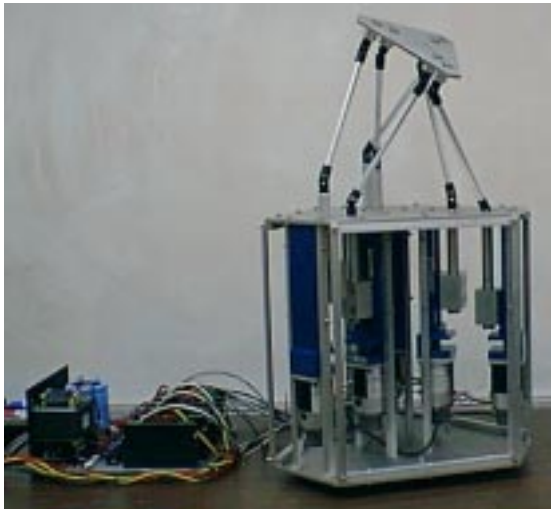

Figure 9. 6-PSU Platform Manipulator Hardware

Six electromechanical ball-screw actuators with 2.54 *mm* (1/10") screw pitch, 101.6 *mm* (4") of travel, and 150 *N* load capacity were selected for the prismatic actuators. Six DC servomotors with PWM servo amplifiers and a 24-volt power supply were selected to transport the moving platform mass over the full range of motion in 1 second. Two-channel, 500 count-per-revolution encoders with quadrature were selected. The combination of the encoder, actuator pitch, and gearing yields feedback resolution of 20,000 encoder counts per inch of actuator travel.

A Multi-Q control board from Quanser Corporation provides the control of the leg servomotors. This system enables closed-loop hardware control in real-time from Matlab's Simulink environment. The Quanser Multi-Q board requires Matlab with Simulink and the Real Time Workshop. It also requires that Visual C++ be installed. This all works together with the Wincon software provided by Quanser. Models built in Simulink can be readily compiled and run for rapid prototyping real-time control.

5. CONTROL ARCHITECTURE

Figure 10 shows the hardware control architecture. The hardware is controlled in inverse pose mode: Given the desired Cartesian pose *X*, calculate active prismatic actuator lengths L_C. The inverse pose solution was presented in Section 3.1. The system may also be controlled in rate mode by implementing resolved-rate control using the Jacobian matrix as presented in Hopkins (2001).

In Fig. 10, L_C is the vector of commanded leg lengths for all prismatic actuators, calculated via inverse pose kinematics from the desired Cartesian pose. L_E is the vector of length errors, the difference between the commanded and measured leg lengths. I_C is the vector of six applied DC servomotor currents, calculated by the proportional-integral-derivative (PID) control law. The Platform Dynamics block is not modeled but is provided by the real-world hardware. X_A and L_A are the actual Cartesian pose and prismatic actuator lengths resulting from the control. L_M are the measured leg lengths, from the encoders' feedback (Length Sensing).
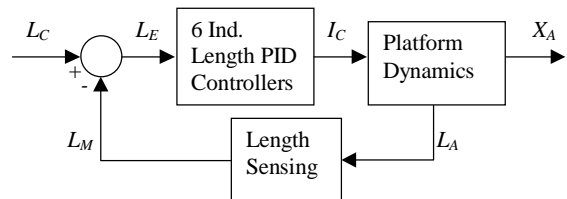

Figure 10. 6-PSU Control Architecture

In the first block of Fig. 10, low-level independent joint control of the six linear actuator lengths is required. The closed-loop feedback joint control diagram for one of the linear actuators is shown in Fig. 11. A disturbance current T_d is given to account for unmodeled platform dynamics.
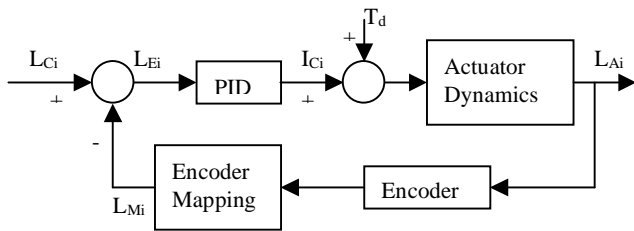
Figure 11. Actuator Length Control Block Diagram

In this manner we achieve coordinated Cartesian control of the platform via linearized independent (but simultaneous) linear actuator control. We have not derived the platform dynamics block in Fig. 10; in fact, the Simulink diagram implementation of Fig. 10 is open at these blocks (the real-world hardware and sensors close the loop). The PID gains have been determined experimentally. We use the Simulink PID block (with approximate derivative to minimize the problems with numerical differentiation). Initially the PID design was performed for individual actuators on the benchtop. Using these gains as a starting point, the next step is to perform the PID design for each actuator within the context of the coupled system dynamics. The PID gains are identical for all six actuators, both on the benchtop and in the manipulator. General control design specifications are smooth motion, low overshoot, plus fast rising and settling times.

6. EXPERIMENTAL RESULTS

The 6-PSU platform system mechatronic design has been completed and the manipulator has been constructed at Ohio University, as shown in Fig. 9. Sample single actuator control and coordinated Cartesian motion experimental results are given in this section.

Figure 12 shows a sample result for hardware linear actuator control on the benchtop (not within the coupled dynamic system). Independent control of all six legs is similar, so only one result is shown. For this case, the actuator length was commanded from the minimum extent to a displacement of 1 inch. As shown in Fig. 12, this command (dotted line) is a step input. The actual control results (solid line) follow the input command well: zero overshoot, zero steady-state error, and a rise time of less than 0.2 *sec* were achieved.
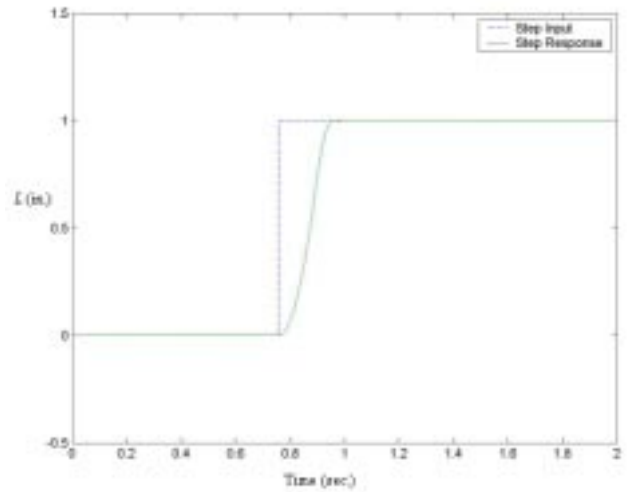

Figure 12. Actuator Length Control

Coordinated Cartesian motion control was performed to demonstrate the six Cartesian translations and rotations, one at a time. The commanded and measured leg actuator lengths for the Cartesian motions are shown in Fig. 13. At the beginning of the time range in Fig. 13, all six actuators move to place the moving platform in the middle of the manipulator workspace (also, at the end, all six actuators return to their minimum extent). In between, sinusoidal-like third-order polynomial Cartesian motions are commanded for $x_H, y_H, z_H, \theta_z, \theta_y, \theta_x$ individually, in turn. Towards the middle of Fig. 13, the unison motion of all six actuators can clearly be seen, providing sinusoidal-like motion in the z direction. Other than this case, the leg lengths are less recognizable for the other five Cartesian motions (we have not even labeled which leg is which); they are shown simply to demonstrate the good agreement between commanded and measured actuator lengths (no discernible difference).

In Fig. 13, the first pair of lobes corresponds to sinusoidal-like x_H motion; the second to y_H, and the third (in unison) to z_H. Furthermore, the fourth pair of lobes corresponds to sinusoidal-like θ_z motion; the fifth to θ_y, and the sixth to θ_x. The amplitude of the translational movements is ±2" from the nominal configuration, and the amplitude of the rotational movements from nominal is ±30°.

Since the commanded and measured leg lengths are indistinguishable to the eye in Fig. 13, Fig. 14 shows the errors between the commanded leg lengths and the measured leg lengths for the same sinusoidal-like Cartesian motions. The magnitude of the error is less than 0.06 *in* over the entire motion time and at most times the error is less than 0.02 *in*. The larger errors occur at times when the manipulator is moving at higher speeds (primarily, during the z_H motion).
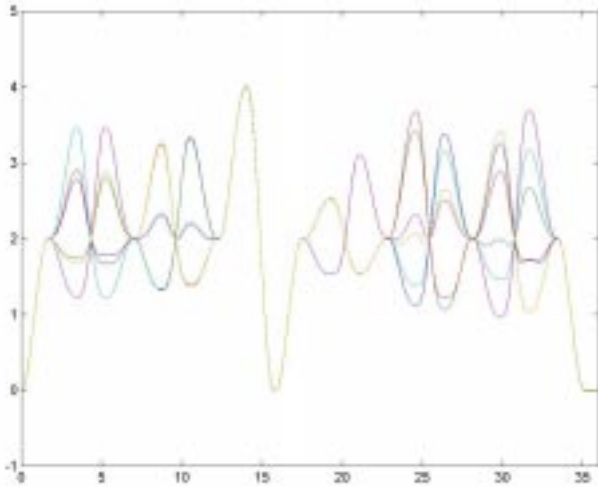
*Figure 13. Coordinated Cartesian Motion Results
Leg Length L (in.) vs. Time (sec)*

We do not show the commanded and measured Cartesian motion results since the actual Cartesian motion is more difficult to measure.   The as-built platform manipulator system is of sufficient stiffness and built with very little backlash and clearances so that we may use forward Cartesian pose kinematics to calculate the actual Cartesian pose given the measured actuator leg lengths.   When we performed this exercise, there was no discernible difference between the commanded and actual (via forward pose kinematics) Cartesian poses, hence this is not shown.
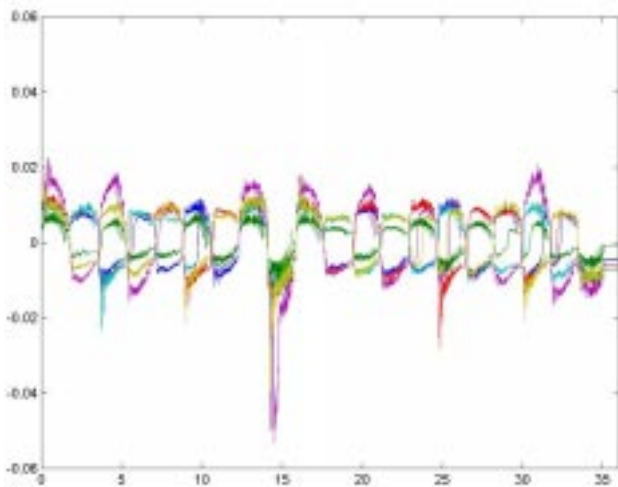

Figure 14. Leg Length Errors (in.) vs. Time (sec)

7. CONCLUSION

This paper has presented a new platform manipulator system for various applications (anything the Stewart/Gough platform can be used for). The six-dof system consists of six identical PSU legs connecting the fixed base and moving platform.   A major improvement over the Stewart/Gough platform is that the active prismatic joints are controlled with respect to the base, hence the actuators need not be articulating as for the Stewart/Gough platform. Compared with the existing *ParaDex* manipulator, our modified 6-PSU manipulator has base and moving platform joint locations mounted on concentric circles, which possesses Jacobian conditioning and workspace benefits over the *ParaDex* design, according to previous literature (Stoughton and Arai, 1993). A hardware system has been designed and constructed at Ohio University, and controller implementation has been accomplished.   Sample single actuator control and coupled Cartesian motion experimental results were presented.

REFERENCES

I.A. Bonev and J. Ryu, 1999, *"Workspace Analysis of 6-PRRS Parallel Manipulators Based on the Vertex Space Concept"*, ASME Design Technical Conferences, DETC99/DAC-8647, Las Vegas, NV, September 12-15, 1999.

J.J. Craig, 1989, Introduction to Robotics: Mechanics and Control, Addison Wesley Publishing Co., Reading, MA.

B. Hopkins, 2001, "Modified ParaDex: Theory and Hardware Implementation of a 6-PSU Parallel Manipulator", MS Thesis, Ohio University.

J.-P. Kim and J. Ryu, 2000, "Closed-Form Dynamics Equations of 6-DOF PUS Type Parallel Manipulators", ASME Design Technical Conferences, 26th Biennial Mechanisms Conference, Baltimore, MD, September 10-13.

 D. Kozlowski and R. Stoughton, 05/30/2001, "ParaDex: A Novel 6-DOF Parallel Manipulator,"
 http://www.sandia.gov/isrc/ParaDex/paradex.html.

J.P. Merlet and C.M. Gosselin, 1991, "New Architecture for a Six-degree-of-freedom Parallel Manipulator," Mechanism & Machine Theory, 26(1): 77-90.

D. Stewart, 1966, "A Platform with Six Degrees of Freedom", Proceedings of the Institute of Mechanical Engineers (London), 180(15): 371-386.

R. Stoughton, and T. Arai, 1993, "A Modified Stewart Platform with Improved Dexterity", IEEE Transactions on Robotics and Automation, 9(2): 166-173.

Y. Wang, W.S. Newman, and R. Stoughton, 2000, "Workspace Analysis of the ParaDex Robot—A Novel, Closed-Chain, Kinematically-Redundant Manipulator." IEEE International Conference on Rob. & Automation, 3: 2392-2397.